Electronic Supplementary Material (ESI) for Chemical Communications.
This journal is © The Royal Society of Chemistry 2022

Supporting Information

Demethylation of Artificial Hydrogenase Agent for Prolonged CO Release and Enhanced Anti-Tau Aggregation Activity

Yun-Chin Wu,[a‡] Yu-Chiao Liu,[b‡] Shu-Wei Tsai,[a] Kai-Ti Chu,[b] Hsin-Jou Chen,[a] Cheng-Yun Wu,[a] Yu-Yi Hsu,[b] Chang-Chih Hsieh,[b] Wang-Jing Liu,[d] Kien Voon Kong,[a*] Ming-Hsi Chiang[bc*]

[a]Department of Chemistry, National Taiwan University, Taipei, 10617, Taiwan

[b]Institute of Chemistry, Academia Sinica, Nankang, Taipei 115, Taiwan

[c]Department of Medicinal and Applied Chemistry, Kaohsiung Medical University, Kaohsiung, 80708, Taiwan

[d]Department of Earth and Life Science, University of Taipei, Taipei 100234, Taiwan

Experimental:

Figure:

1. General methods

All reactions were carried out using standard Schlenk and vacuum-line techniques under an atmosphere of purified N_2. All commercially available chemicals were of ACS grade and used without further purification. Solvents were of ACS grade and purified as follows: dichloromethane (CH_2Cl_2) was distilled from CaH_2 under N_2; tetrahydrofuran (THF) was distilled from sodium/benzophenone under N_2; hexane was distilled from sodium under N_2. Deuterated solvents obtained from Merck were distilled over 4 Å molecular sieves under N_2 prior to use. [(μ-bdt)$Fe_2(CO)_6$] (bdt = 1,2-benzenedithiolate) was prepared according to reported procedures.[1] Infrared spectra of complexes dissolved in organic solvents were recorded on a PerkinElmer Spectrum One using a 0.05 mm CaF_2 cell. ^{1}H and ^{31}P{^{1}H} NMR spectra were recorded on a Bruker AV-500 or DRX-500 spectrometer operating at 500 and 202.49 MHz,

respectively. UV-vis absorption spectra were recorded on a Varian Cary 5000 spectrophotometer using a 1 cm quartz cell.

2. Synthesis of $[Fe_2(CO)_5(\mu,\kappa^2\text{-bdt})(\mu\text{-}PPh_2)(S\text{-}Me)]$ (Me = CH_3; Fe-CORM).

The complex was synthesized according to a modified method.[11-12] To a red THF solution (50 mL) of $[(\mu\text{-bdt})Fe_2(CO)_6]$ (500 mg, 1.19 mmol) was added freshly prepared $NaPPh_2$ (1.19 mmol) in the THF solution. The solution was stirred overnight. To this solution was added 300 μL of CH_3I (4.8 mmol) solution. An immediate color change from dark-green to orange-red was observed. The solution was stirred at room temperature and monitored by FTIR. The solvent was removed under vacuum upon the completion of the reaction. CH_2Cl_2 (30 mL) was added to dissolve the orange-red solid, and the solution was filtered through celite (Celite® S, Sigma-Aldrich). The filtrate was concentrated to minimal amount and the orange-red solid product was obtained upon addition of hexane. The yield of the product was 83%. The sample was recrystallized from the CH_2Cl_2/hexane solution at 253 K prior to biomedical measurements. IR (THF, cm^{-1}): ν_{CO} 2029 (m), 1987 (vs), 1955 (s), 1929 (m). ^1H NMR (500 MHz, $CDCl_3$, ppm): 2.78 (s, 3H, SC*H*$_3$), 7.25-7.76 (m, 14H, $S_2C_6H_4$, $P(C_6H_5)_2$). ^{31}P NMR (202.49 MHz, $CDCl_3$, ppm): 149.73 (s) ppm. FAB^+-MS: m/z 591.9 $\{M\}^+$. Anal. Calcd for $C_{24}H_{17}Fe_2O_5PS_2$: C, 48.68; H, 2.89. Found: C, 48.75; H, 3.10.

3. Mass spectrometry, EA and GC analysis

Mass spectral analyses were performed on a JEOL JMS-700 double focusing mass spectrometer at the Mass Spectrometry Center in the Institute of Chemistry, Academia Sinica. Elemental analyses (EA) were performed on a Thermo Fisher EA1112 elemental analyzer. CO gas was detected using an Agilent 7890 GC system equipped with a thermal conductivity detector (TCD) and fitted with a Restek ShinCarbon ST column (100/120 mesh, 2 m, 1/16 in. OD, 1.0 mm ID). Carrier gas was helium. Photolysis of $[Fe_2(CO)_5(\mu,\kappa^2\text{-bdt})(\mu\text{-}PPh_2)(S\text{-}Me)]$ (Fe-CORM) was conducted using a Kessil lamp (PR-160, λ_{max} = 427 nm). Fe-CORM (10 mg, 0.017 mmol) was dissolved in 8 mL of ethanol solution. The solution was irradiated with the light source under nitrogen. The distance between the solution and the light source was 35 cm. The reaction was monitored by FTIR. The gaseous sample in the headspace of the reactor was analyzed by gas chromatography-thermal conductivity detector (GC-TCD).

4. Computational methods

All density functional theory (DFT) calculations including full geometry optimizations and Raman spectra were performed on Fe-CORM and $[Fe_2(CO)_5(\mu,\kappa^2\text{-bdt})(\mu\text{-}PPh_2)]^-$ (denoted as Fe-bdtPPh$_2^-$) by using a hybrid functional B3LYP[2-3] on *Gaussian 09*.[4] The effective core potential and associated basis set of LANL2DZ were used for the Fe atom,[5] and the 6-31G(d,p) basis set was used for O, S, C and H atoms. All thermochemical and spectroscopic properties were calculated under the solvent effect by using the polarizable continuum model (CPCM) for H_2O.[6-8] Time-dependent DFT calculations[9-10] were employed to investigate vertical electronic transitions using the B3LYP/LANL2DZ combination.

5. Raman experiments

The Raman spectral measurements were carried out using a Renishaw In Via Raman (UK) microscope with a Peltier cooled CCD detector and an excitation wavelength at 633 nm, where the laser excitation was directed onto the sample via a 50× objective lens (with a confocal pinhole 25 μm in diameter), and the exposure time was set at 10 s for all of the measurements. All Raman spectra were processed using WiRE 4.3 software. Before each measurement, the instrument was calibrated using the standard Raman spectrum of silicon, whose Raman peak is centered at 520 cm^{-1}. For each sample, SERS spectra (n = 10) were acquired over a 60 × 60 μm area with a 10-μm interval. The CO spectra were presented at baseline using a polynomial multipoint fitting function and curve fitting function provided by the Renishaw WiRE 4.3 software. Cell samples was then irradiated by a Kessil PR160L 45 W 427 nm at 50 % light intensity with 6 cm distance from sample for 1 h. To reduce the heat generation, the performed under air laminar flow condition.

6. Fabrication of nanopillar substrate

Four-inch p-type single side polished <100> wafers were used. Etching is conducted in an Advanced Silicon Etcher. Nanopillars were formed using an ion etching method. After step, the nanopillars were exposed to argon plasma for 1 min to completely remove the etchant gas residuals and the decomposition products. A chromium adhesion layer is evaporated onto the Si nanopillar structure. Finally, gold was deposited on the heads of the nanopillars by electron beam evaporation.

7. Cell culture

Neuro-2a cells were purchased from Bioresource Collection and Research Center (BCRC) in Taiwan. Cells were cultured in Minimum Essential Medium α (α-MEM) with 10% fetal bovine serum (FBS) and 1% penicillin/streptomycin in sterile 25 cm^2 cell culture flasks in a humidified incubator with 5% CO_2 and 95% air at 37°C.

8. Cell viability assay

Cells were seeded in 96-well plates at the density of 5×10^3/100 μL and incubated for 24 h to reach exponential growth. Afterward, cells were treated with Fe-CORM at concentrations ranging from 0.05 μM to 1000 μM, respectively. One plate was irradiated with light for 1 hour, and the other plate was used under dark condition as a control. Cell viability was measured via ReadyProbes™ Cell Viability Imaging Kit, Blue/Green. 1 μL NucBlue Live reagent (staining the nuclei of all cells) and 1 μl NucGreen Dead reagent (staining only the nuclei of dead cells with compromised plasma membranes) were added into each well. The live cell images were acquired on a Zeiss AxioImager Z1 epifuorescence microscope. The green fluorescence intensity was recorded at 488 nm by a microplate reader (SynergyTM H1) with an excitation at 442 nm. Each replicate included one background control (pure medium). All experiments were performed in n = 3 technical replicates. The cell viability was calculated by the equation:

$$\%\,Viable\ cells = \left(1 - \frac{Number\ of\ dead\ cells\ in\ a\ fixed\ area\ (cell\ numbers\ with\ GFP\ fluorescenc}{Total\ number\ of\ cells\ in\ a\ fixed\ area\ (cell\ numbers\ with\ DAPI\ fluorescen}\right.$$

9. Carbon monoxide detection

Neuro-2a cells were seeded in 96-well plates for one night before live cell imaging experiments. Before detection of exogenous CO released by Fe-CORM, cells were pretreated with COP-1 and $PdCl_2$ (1 μM each) for 1 hour at 37 °C. Fe-CORM (10 μM) was then added and diffused for 1 hour at 37 °C. After exposure to light irradiation for 1 hour, exogenous CO would release by Fe-CORM in cells in 1 hour. The live cell images were acquired on a Zeiss AxioImager Z1 epifuorescence microscope. The green fluorescence intensity was recorded at 488 nm by a microplate reader (SynergyTM H1) with an excitation at 442 nm indicated the intracellular CO level produced by Fe-CORM.

10. Tau protein aggregation and amyloid-beta (Aβ) plaque assay

Neuro-2a cells were grown in 96-well plates. Okadaic acid (OA) was dissolved in ethanol to a concentration of 124 μM as a stock solution. The stock solution was diluted with α-MEM to 60 nM prior to use. When the cell density reached 80%, the cells were pre-incubated with BioTracker Tau filaments pFTAA Live cell dye (3 μM) for 1 hour at 37 °C. After washing with PBS buffer for three times, cells were treated with Fe-CORM (0.05 μM to 10 μM) and exposed to light irradiation for 1 hour and then incubated overnight. Another plate was used under dark condition as a control. The second day, OA (60 nM) was added and incubated for another 12 hours at 37°C. The live cell images were acquired on a Zeiss AxioImager Z1 epifuorescence microscope. The green fluorescence intensity was recorded at 488 nm by a microplate reader (SynergyTM H1) with an excitation at 442 nm. Each replicate included one background control (pure medium). All experiments were performed in $n = 3$ technical replicates. The tau NFTs and Aβ plaques amount was calculated by the equation:

$$\%\ tau\ NFTs\ and\ A\beta\ plaques\ amount = \left(\frac{Number\ of\ cells\ producing\ tau\ NFTs\ and\ A\beta\ plaques\ in\ a\ fixed\ area\ (cell\ numbers\ with}{Total\ number\ of\ cells\ in\ a\ fixed\ area\ (cell\ numbers\ with\ DAPI\ fluoresce}\right) \times 100$$

11. Statistical analysis

Each data and error bars were calculated from three independent experiments. Data was analyzed for significant differences between the treated and control groups in the absence or presence of light irradiation by student's t-test. GraphPad Prism was used to perform statistical tests with statistical significance set to a $^{*}P < 0.05$; $^{**}P < 0.01$.

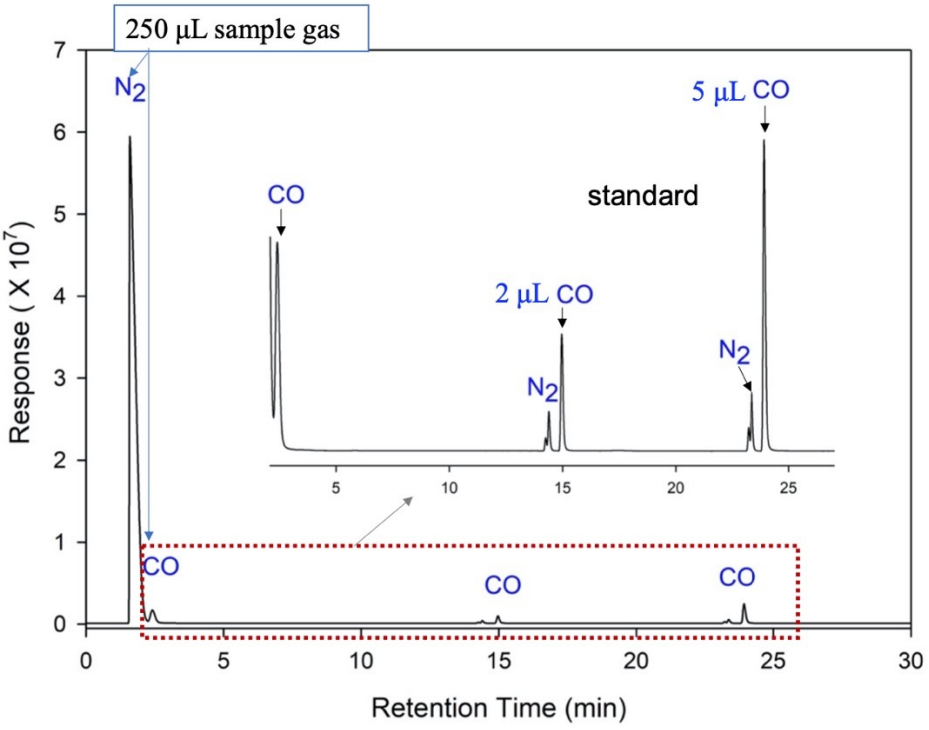

Figure S1. GC analysis of the gaseous sample from the photolysis of Fe-CORM in ethanol solution. The following 2 CO signals are the standard for calibration. The 250-µL sample gas is calculated to contain 4.63 µL of CO.

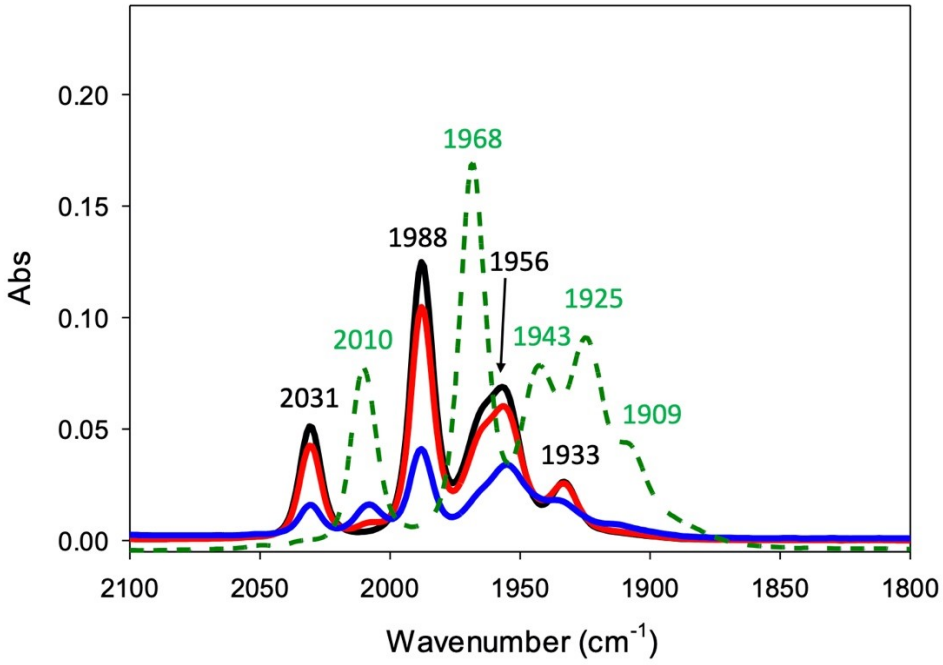

Figure S2. Changes of FTIR spectra of the photolysis of Fe-CORM in ethanol solution: 0 (black), 1 (red) and 5 h (blue). The FTIR profile of $[Fe_2(CO)_5(\mu,\kappa^2\text{-bdt})(\mu\text{-}PPh_2)]^-$ is shown in a green dash line for comparison.

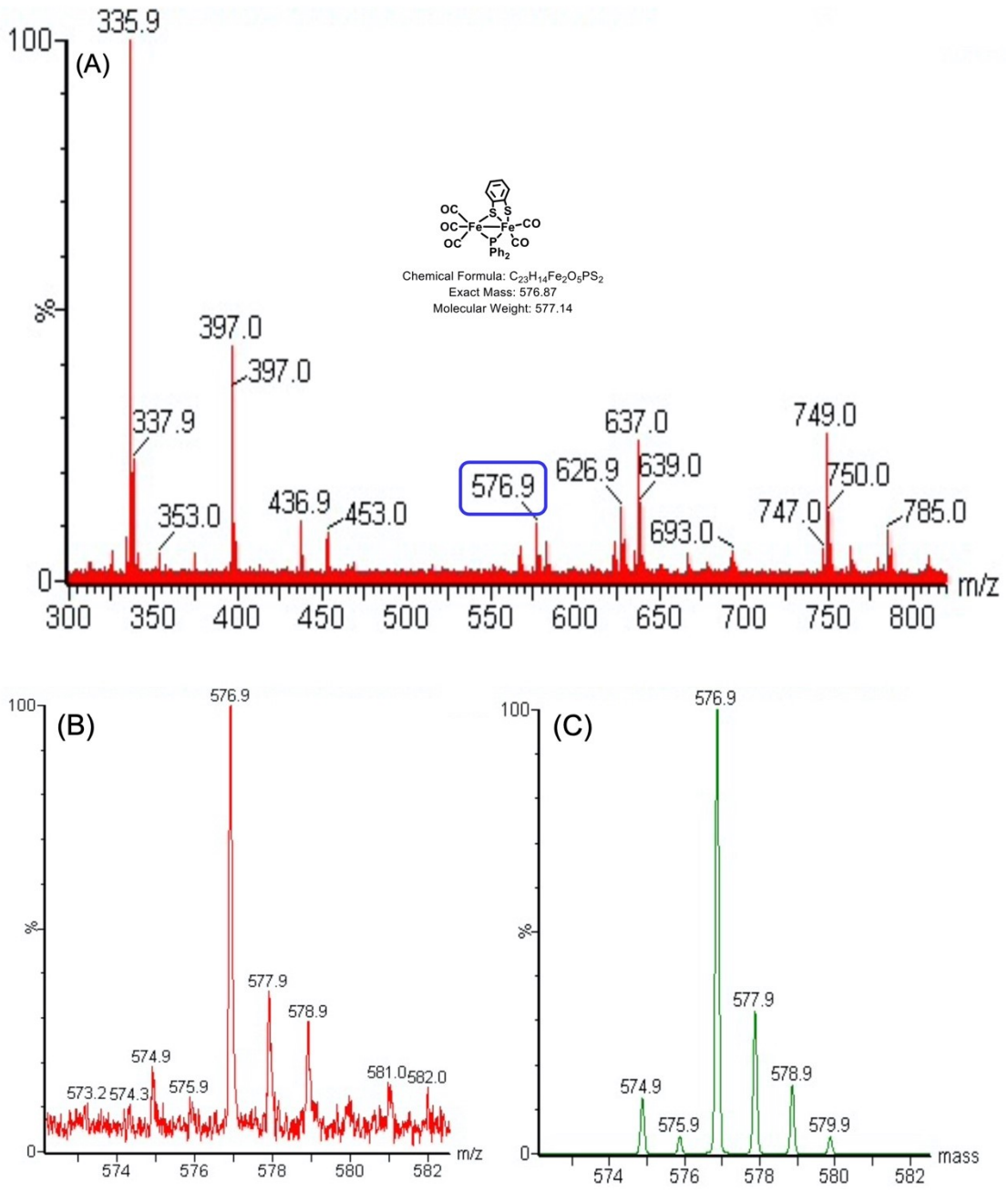

Figure S3. Negative mode ESI-MS spectra of photolysis products (5 hr), show the presence of $[Fe_2(CO)_5(\mu,\kappa^2\text{-bdt})(\mu\text{-}PPh_2)]^-$ (m/z = 576.87): full spectrum (A), expanded spectrum (B) and theoretical isotopic distribution patterns (C).

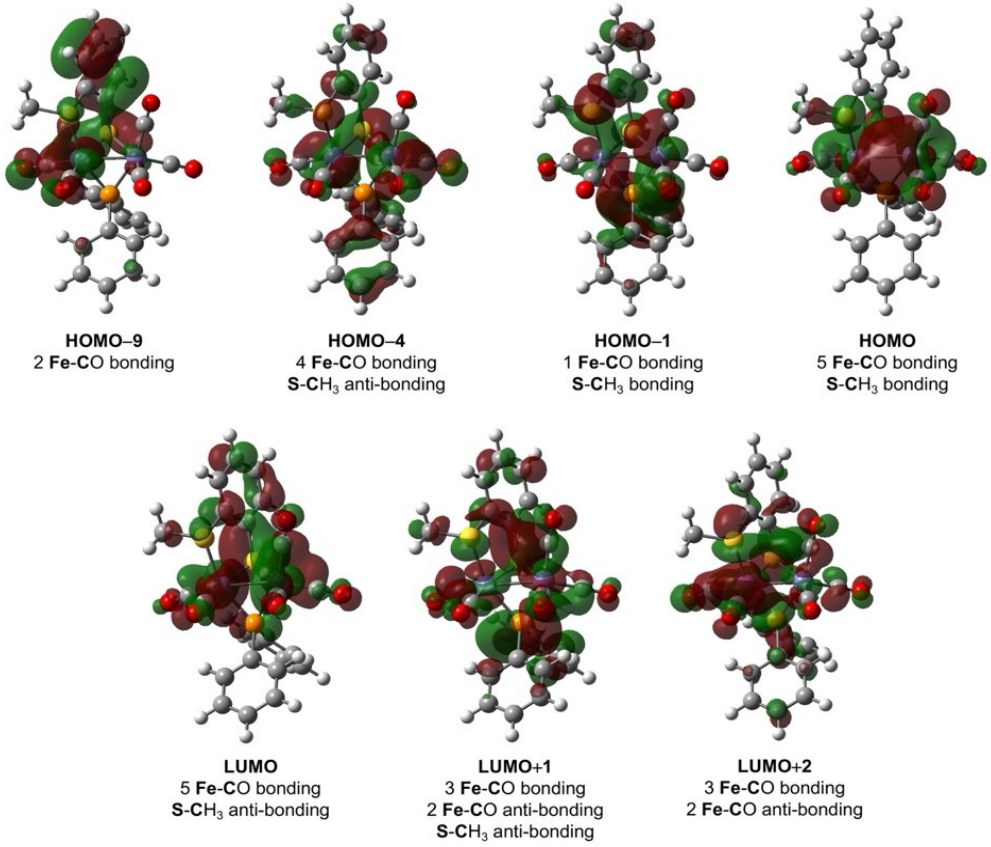

Figure S4. MOs related to the electronic transitions for Fe-CORM.

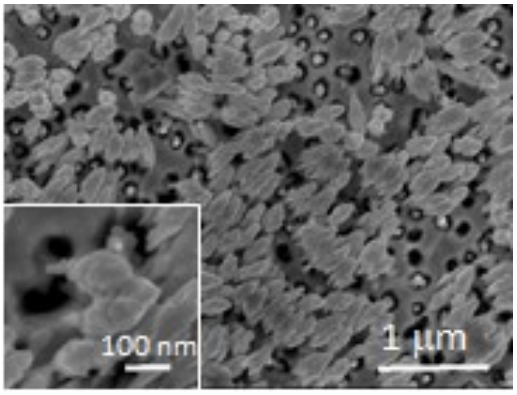

Figure S5. SEM image of nanopillars substrate. SEM image shows a high density of the nanopillars over a large area.

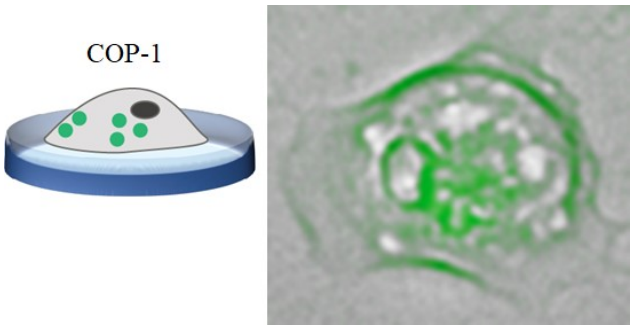

Figure S6. The fluorescence CO sensing using COP-1.

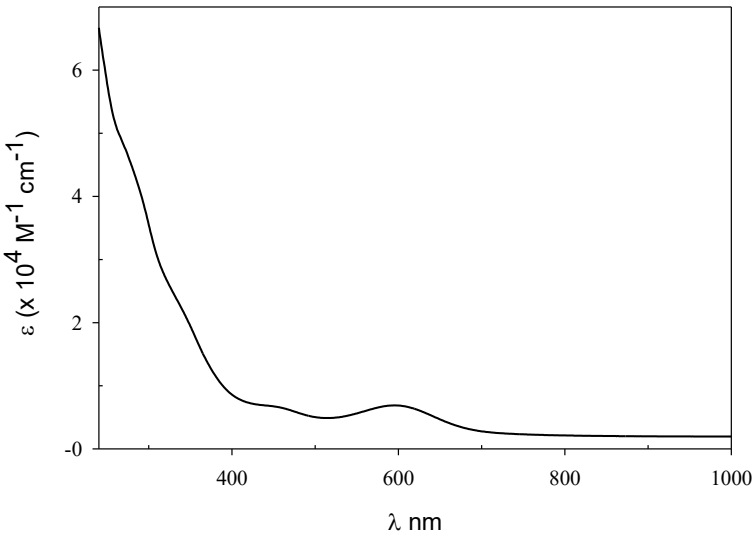

Figure S7. The UV-vis spectrum of Fe-bdtPPh$_2^-$ in THF solution.

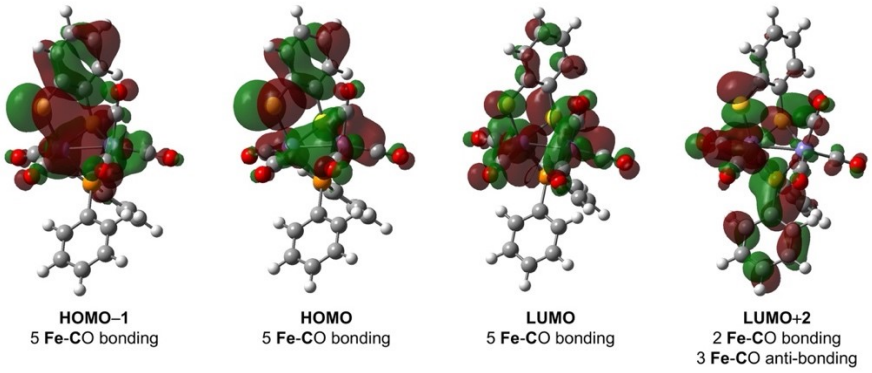

Figure S8. MOs related to the electronic transitions for Fe-bdtPPh$_2^-$.

Computational results on Raman shifts

The assignment of every state during the process of CO-releasing was performed on the basis of the combined results of the in situ spectroscopic and DFT calculation studies. The Raman signals for the selected optimized structures were consistent with the corresponding results of the in-situ measurements. A linear relationship between the computed and measured data for all species is obtained.

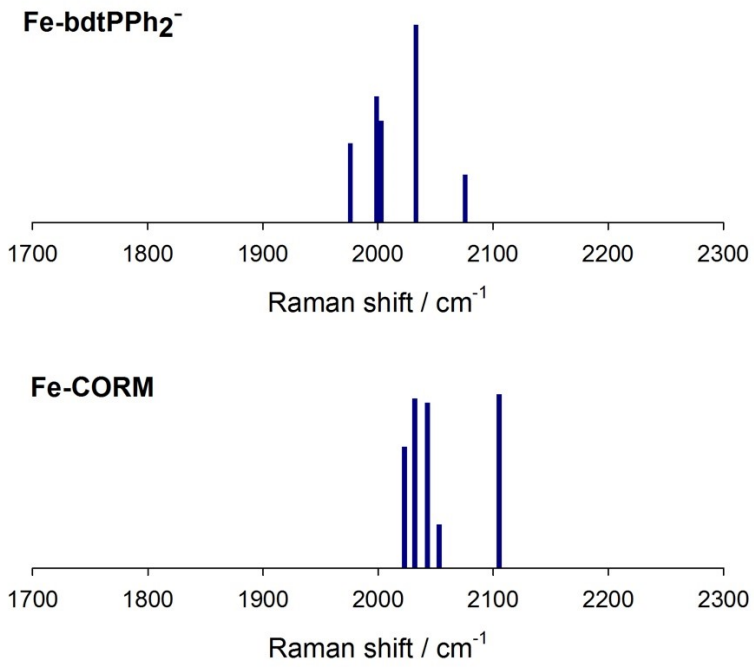

Figure S9. DFT-calculated Raman spectra of Fe-bdtPPh$_2^-$ and Fe-CORM.

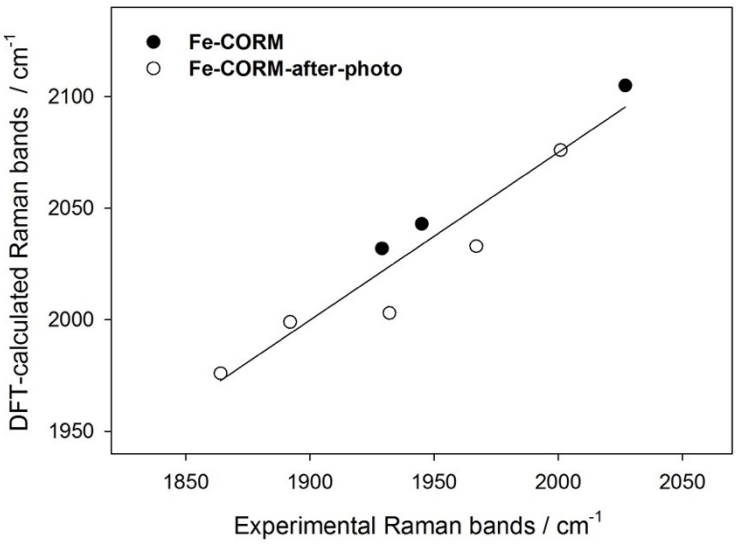

Figure S10. Linear relationship (R^2 = 0.91) between experimental and DFT-calculated Raman bands for Fe-CORM and Fe-CORM-after-photo.

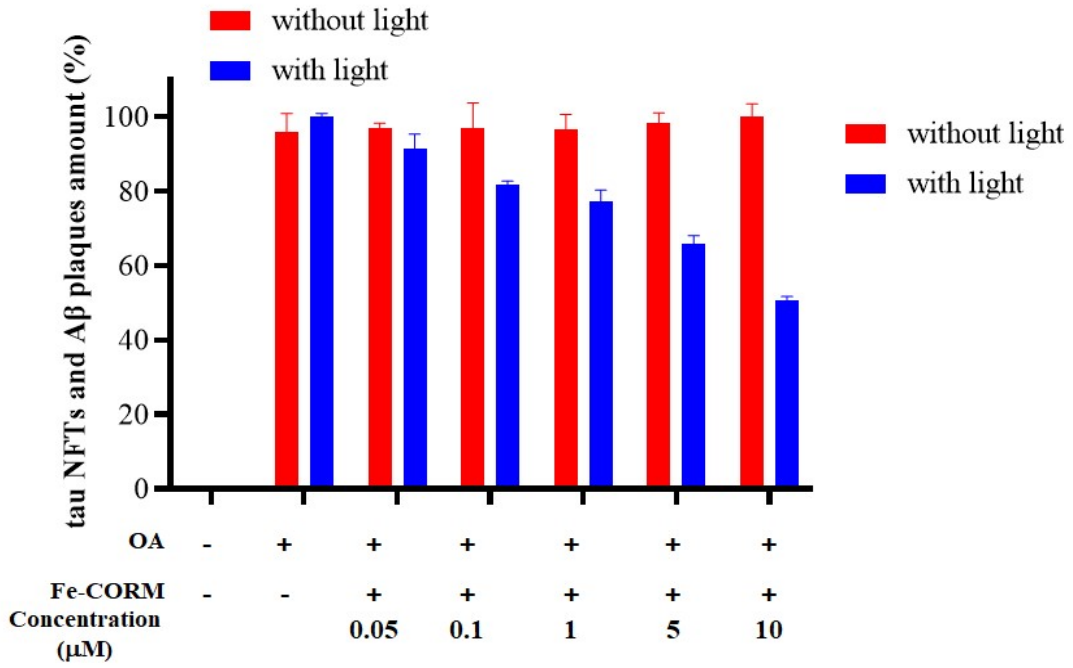

Figure S11. Student's t-tests for the performance of anti-tau aggregation show significant differences in performance between the presence and absence of light.

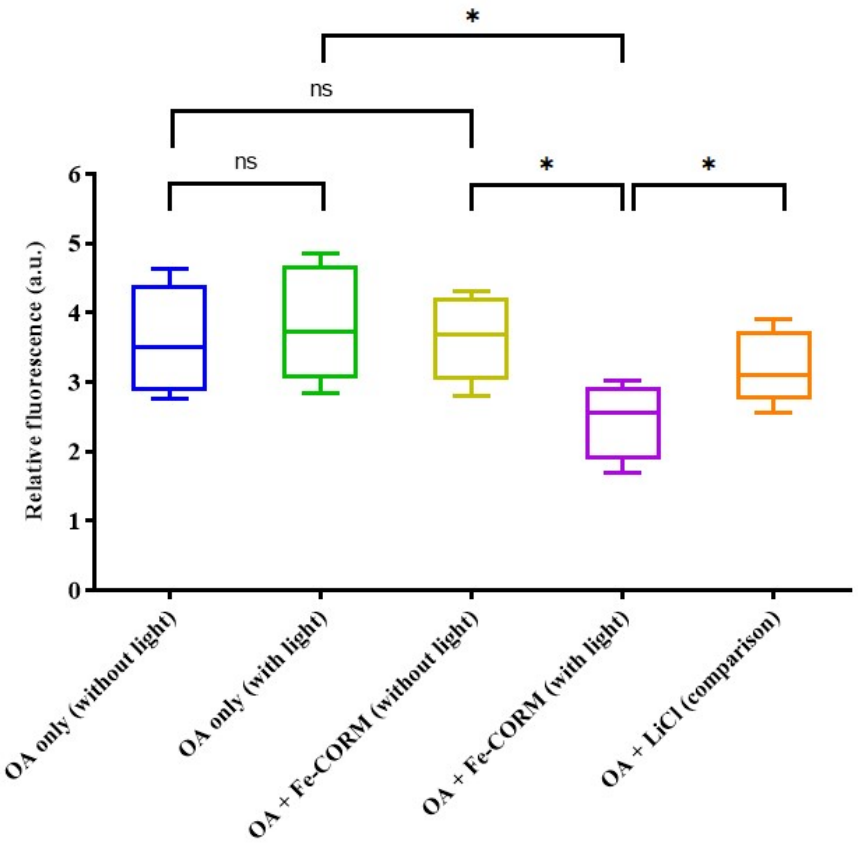

Figure S12. The relative fluorescence intensity of tau NFTs and Aβ plaques between OA only (without/with light), OA + Fe-CORM (without/with light), and OA + lithium chloride (for comparison).

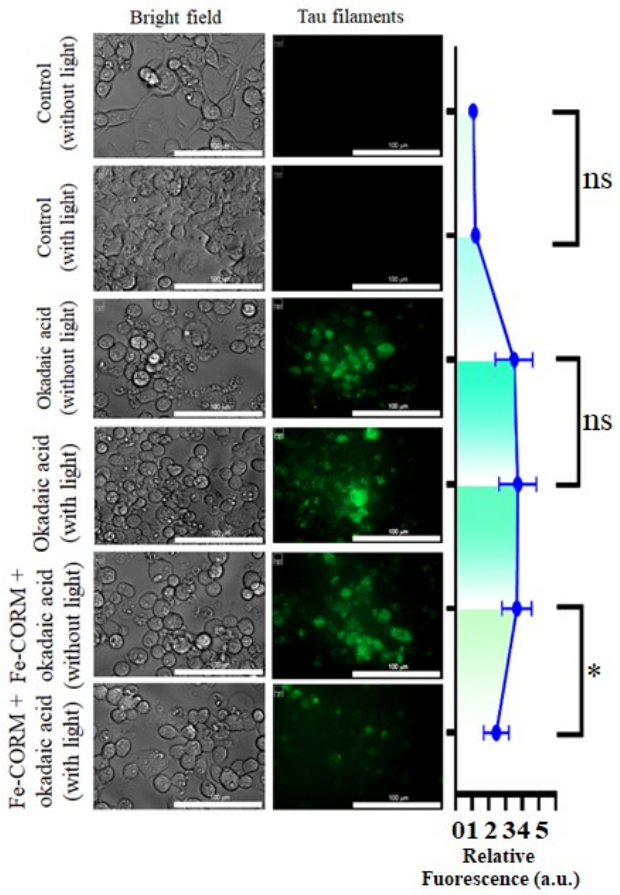

Figure S13. Fluorescence imaging of tau aggregation (OA = 60 nM; Fe-CORM = 10 μM; 30 min light irradiation.

Table S1. Summary of experimental and DFT-calculated Raman shifts.

Experimental Raman bands (cm^{-1})	
Fe-CORM	2027, 1945, 1929
Fe-CORM-after-photo	2001, 1967, 1932, 1892, 1864
DFT-calculated Raman bands (cm^{-1})	
Fe-CORM	2105, 2053, 2043, 2032, 2023
Fe-bdtPPh$_2^-$	2076, 2033, 2003, 1999, 1976

*Due to the low S/N ratio from experimental results for Fe-CORM, three DFT-calculated bands with highest intensity are chosen for comparison.

Table S2. Cartesian coordinates of DFT geometry-optimized species.

Fe-CORM

Symbol	X	Y	Z
Fe	-0.451574	-0.745137	-0.898319
Fe	-0.172061	-0.008622	1.533435
S	-1.303551	1.25872	-0.128241
S	-2.608905	-1.642945	-0.741212
P	1.422005	0.147734	-0.078973
C	0.251073	-2.382165	-0.87591
C	-0.345809	-0.446269	-2.633812
C	-1.708534	-0.441765	2.346692
C	0.424425	1.251438	2.642342
C	0.575642	-1.485476	2.154353
C	-3.069417	0.9878	-0.009582
C	-3.895864	2.058551	0.362862
H	-3.445059	3.021348	0.582282
C	-5.276146	1.89057	0.448109
H	-5.902177	2.729247	0.737568
C	-5.852785	0.648687	0.169393
H	-6.927133	0.51264	0.244301
C	-5.042234	-0.424641	-0.194445
H	-5.48269	-1.398064	-0.388211
C	-3.657641	-0.251249	-0.300585
C	2.996317	-0.799899	-0.000163
C	3.533722	-1.349343	-1.175645
H	3.000821	-1.236948	-2.11557
C	4.744571	-2.040451	-1.145598
H	5.145883	-2.463917	-2.061851
C	5.435981	-2.190301	0.05854
H	6.377671	-2.731055	0.082173
C	4.912182	-1.646284	1.231707
H	5.443564	-1.76204	2.171955
C	3.698962	-0.955883	1.204212
H	3.298321	-0.5407	2.123734
C	2.005085	1.823366	-0.589926
C	2.958069	2.489931	0.200479
H	3.35146	2.01404	1.093841
C	3.409464	3.76018	-0.151315

H	4.144231	4.261649	0.472176
C	2.917327	4.387012	-1.299278
H	3.269145	5.377703	-1.572547
C	1.975157	3.733681	-2.092481
H	1.590148	4.211524	-2.988868
C	1.521431	2.459554	-1.742017
H	0.790434	1.962963	-2.368504
O	0.680001	-3.453371	-0.88014
O	-0.245744	-0.25491	-3.770653
O	-2.674129	-0.718021	2.913606
O	0.8343	2.040074	3.378024
O	1.032278	-2.452503	2.592468
C	-3.214942	-1.991832	-2.440295
H	-2.58533	-2.79273	-2.832993
H	-4.250556	-2.332829	-2.400508
H	-3.124883	-1.104913	-3.068412

Fe-bdtPPh$_2^-$

Symbol	X	Y	Z
Fe	-0.504475	-0.62128	-1.101981
Fe	-0.281083	-0.308547	1.491753
S	-1.463873	1.146782	-0.015819
S	-2.632509	-1.583082	-1.345832
P	1.318792	0.152929	-0.057937
C	0.189187	-2.228293	-1.400072
C	-0.427026	-0.016646	-2.738868
C	-1.83475	-0.861304	2.165679
C	0.261096	0.73974	2.806324
C	0.409277	-1.904805	1.742819
C	-3.2149	0.809991	-0.065861
C	-4.100544	1.762022	0.462039
H	-3.694269	2.669146	0.901941
C	-5.475479	1.550418	0.427933
H	-6.153046	2.292333	0.84205
C	-5.971874	0.371987	-0.146531
H	-7.04419	0.192254	-0.180189
C	-5.102555	-0.57132	-0.679184

H	-5.491669	-1.482207	-1.125659
C	-3.7032	-0.376772	-0.655799
C	2.929101	-0.752658	-0.097654
C	3.548304	-1.023313	-1.329183
H	3.058975	-0.718639	-2.250169
C	4.776485	-1.682346	-1.381856
H	5.237689	-1.887384	-2.344657
C	5.407667	-2.084323	-0.202253
H	6.362686	-2.601959	-0.242927
C	4.801873	-1.824897	1.027468
H	5.282107	-2.140942	1.949999
C	3.571337	-1.165664	1.079286
H	3.101222	-0.975851	2.039068
C	1.912856	1.896548	-0.257566
C	2.869933	2.426239	0.625596
H	3.268981	1.804804	1.42212
C	3.315645	3.740339	0.494715
H	4.054964	4.130218	1.190093
C	2.81042	4.555343	-0.522141
H	3.15579	5.581164	-0.623345
C	1.860544	4.042516	-1.405016
H	1.460541	4.666593	-2.200148
C	1.416739	2.723682	-1.275997
H	0.67938	2.334091	-1.968107
O	0.615306	-3.281471	-1.616855
O	-0.373982	0.383372	-3.826386
O	-2.828373	-1.223166	2.63143
O	0.663551	1.354964	3.706807
O	0.849095	-2.953721	1.988508

References:

1. Cabeza, J. A.; Martínez-García, M. A.; Riera, V.; Ardura, D.; García-Granda, S., Binuclear Iron(I), Ruthenium(I), and Osmium(I) Hexacarbonyl Complexes Containing a Bridging Benzene-1,2-dithiolate Ligand. Synthesis, X-ray Structures, Protonation Reactions, and EHMO Calculations. *Organometallics* **1998**, *17* (8), 1471-1477.

2. Becke, A. D., DENSITY-FUNCTIONAL THERMOCHEMISTRY .3. THE ROLE OF EXACT EXCHANGE. *J. Chem. Phys.* **1993**, *98* (7), 5648-5652.

3. Lee, C. T.; Yang, W. T.; Parr, R. G., Development of the colle-salvetti correlation-energy formula into a functional of the electron-density. *Physical Review B* **1988**, *37* (2), 785-789.

4. Frisch, M. J.; Trucks, G. W.; Schlegel, H. B.; Scuseria, G. E.; Robb, M. A.; Cheeseman, J. R.; Scalmani, G.; Barone, V.; Mennucci, B.; Petersson, G. A.; Nakatsuji, H.; Caricato, M.; Li, X.; Hratchian, H. P.; Izmaylov, A. F.; Bloino, J.; Zheng, G.; Sonnenberg, J. L.; Hada, M.; Ehara, M.; Toyota, K.; Fukuda, R.; Hasegawa, J.; Ishida, M.; Nakajima, T.; Honda, Y.; Kitao, O.; Nakai, H.; Vreven, T.; J. A. Montgomery, J.; Peralta, J. E.; Ogliaro, F.; Bearpark, M.; Heyd, J. J.; Brothers, E.; Kudin, K. N.; Staroverov, V. N.; Kobayashi, R.; Normand, J.; Raghavachari, K.; Rendell, A.; Burant, J. C.; Iyengar, S. S.; Tomasi, J.; Cossi, M.; Rega, N.; Millam, J. M.; Klene, M.; Knox, J. E.; Cross, J. B.; Bakken, V.; Adamo, C.; Jaramillo, J.; Gomperts, R.; Stratmann, R. E.; Yazyev, O.; Austin, A. J.; Cammi, R.; Pomelli, C.; Ochterski, J. W.; Martin, R. L.; Morokuma, K.; Zakrzewski, V. G.; Voth, G. A.; Salvador, P.; Dannenberg, J. J.; Dapprich, S.; Daniels, A. D.; Farkas, Ö.; Foresman, J. B.; Ortiz, J. V.; Cioslowski, J.; Fox, D. J. *Gaussian 09*, Revision D.01; Gaussian, Inc.: Wallingford, CT, 2009.

5. Hay, P. J.; Wadt, W. R., Ab initio Effective Core Potentials for Molecular Calculations - Potentials for the Transition-Metal Atoms Sc to Hg. *J. Chem. Phys.* **1985**, *82* (1), 270-283.

6. Miertuš, S.; Scrocco, E.; Tomasi, J., Electrostatic interaction of a solute with a continuum. A direct utilizaion of AB initio molecular potentials for the prevision of solvent effects. *Chem. Phys.* **1981**, *55* (1), 117-129.

7. Miertuš, S.; Tomasi, J., Approximate evaluations of the electrostatic free energy and internal energy changes in solution processes. *Chem. Phys.* **1982**, *65* (2), 239-245.

8. Cossi, M.; Barone, V.; Cammi, R.; Tomasi, J., Ab initio study of solvated molecules: a new implementation of the polarizable continuum model. *Chem. Phys. Lett.* **1996**, *255* (4), 327-335.

9. Bauernschmitt, R.; Ahlrichs, R., Treatment of electronic excitations within the adiabatic approximation of time dependent density functional theory. *Chem. Phys. Lett.* **1996**, *256* (4), 454-464.

10. Stratmann, R. E.; Scuseria, G. E.; Frisch, M. J., An efficient implementation of time-dependent density-functional theory for the calculation of excitation energies of large molecules. *J. Chem. Phys.* **1998**, *109* (19), 8218-8224.

11. Liu, Y.-C.; Chu, K.-T.; Jhang, R.-L.; Lee, G.-H.; Chiang, M.-H., [FeFe] hydrogenase active site modeling: a key intermediate bearing a thiolate proton and Fe hydride. *Chem. Commun.* **2013**, *49* (42), 4743-4745.

12. Chung, M.-W.; Liu, Y.-C.; Yen, T.-H.; Chiang, M.-H., Bilayer Vesicles as a Noncovalent Immobilization Platform of Electrocatalysts for Energy Conversion in Neutral Aqueous Media. *ChemElectroChem* **2018**, *5* (1), 20-24.